CHEMISTRY OF MATERIALS

ARTICLE

pubs.acs.org/cm

Facile Synthesis of PtNi Intermetallic Nanoparticles: Influence of Reducing Agent and Precursors on Electrocatalytic Activity

Brian M. Leonard,[‡] Qin Zhou,[†] Diane Wu,[†] and Francis J. DiSalvo*[,†]

[†]Department of Chemistry and Chemical Biology, Cornell University, Ithaca, New York 14853, United States

[‡]Department of Chemistry, University of Wyoming, Laramie, Wyoming 82071, United States

Supporting Information

ABSTRACT: In this paper, a nonaqueous synthesis of PtNi nanoparticles is presented using multiple reducing agents and metal precursors. Through this investigation, it was found that all the species present in solution have an impact on the resulting nanoparticles. Metal precursor choice has a major effect on the resulting nanoparticles and their behavior. When using acetylacetonate (acac) precursors, the acac ligands bind tightly with the resulting metal particles and cannot be easily removed through washing. After annealing to nucleate the intermetallic phase, these ligands decompose into a carbonaceous coating rendering the particles inactive toward formic acid oxidation. This led to the development of a chloride precursor Li_2NiCl_4, not previously used for synthesis of inorganic nanoparticles, which is soluble in ether solvents unlike $NiCl_2$ and many other metal chlorides. Using the lithium metal chloride as a precursor, the organic content of the nanoparticle products is greatly reduced as seen by lower weight losses in TGA, TEM imaging, lower intermetallic formation temperatures, and greatly enhanced catalytic activity for formic acid oxidation. Additionally, by changing the alkali metal of an alkali metal alkylborohydride reducing agent and thus the resulting salt byproduct, the particle size of the resulting intermetallic nanoparticles can be controlled. These new Li_xMCl_y precursors and synthesis techniques have opened the door to the synthesis of a broad range of intermetallic Pt−M nanoparticles and will allow their study as electrocatalysts.

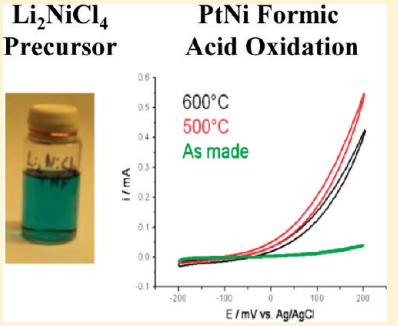

KEYWORDS: intermetallic, nanomaterials, PtNi, fuel cell, electrocatalyst, formic acid oxidation

INTRODUCTION

Fuel cells are very promising energy conversion devices that can in theory convert chemical energy into electrical energy much more efficiently than currently used heat engine technologies.[1,2] The efficiency of fuel cells is not limited by the Carnot principle and can potentially have efficiencies close to 100% of the available free energy. In reality, each of the different fuel cell technologies is complex, and achieving the efficiency and reliability required for commercial applications is still a challenging task. In this investigation, the focus is on challenges that are specific to proton exchange membrane fuel cells (PEMFC) that operate at or near room temperature. There are many materials limitations in the current PEMFCs. For example, better catalyst materials need to be found with higher activity, less sensitivity to poisoning, longer lifetimes, and lower cost.[3,4] Further, it is desirable to also be able to use carbon containing fuels, but, except for formic acid and methanol, there are no catalysts that allow the complete oxidation of the fuel, especially at the desired rates. By alloying Pt with a secondary metal, formic acid and methanol can be oxidized, but at rates that are still too small to attain the desired power densities for many applications.[5−7] Alloying can also reduce the cost of the catalyst, can result in considerable improvements in tolerance to CO poisoning, and consequently is a major area of research. Atomically ordered alloys, usually referred to as intermetallic compounds or just intermetallics for short, have also shown significant improvements in activity or poison tolerance over platinum and are frequently more stable than disordered alloys, due to the higher free energies of formation of intermetallics relative to alloys.[8−16]

A current challenge is to be able to readily form chemically homogeneous intermetallic nanoparticles, as will be necessary for high reaction rates. The highest rates per unit mass of (typically expensive) catalysts are of course obtained if the materials are in the form of nanoparticles. The formation of intermetallic phases as a high surface area nanomaterial is quite challenging in the general case, but a few examples have been reported.[17−20] Many of the reported synthesis methods utilize surface stabilizing agents to help keep the particle size small and close to monodisperse. The problem is that these surface stabilizing agents block the surface of the nanoparticles which often renders them catalytically inactive (poisoned). These stabilizing agents can sometimes be removed by heating or oxidation post synthesis, but the residue from these organic molecules, especially sulfur based compounds, may remain bound to the surface of the particles and continue to poison the catalyst. In some cases, the surfactant can be removed by electrochemical cycling at high potentials, but this process may cause leaching of the second metal.[21] Thus there is a demand for developing synthetic

Received: August 30, 2010
Revised: January 3, 2011
Published: February 04, 2011

methods that avoid the use of surfactants, so that the particles will be active and also readily bind to an appropriate catalyst support.

Additionally, inclusion of very oxophilic metals, such as Ti, V, and Nb, in Pt−M intermetallics further complicates the synthesis procedure.[22] Here we focus on the reduction of metal precursors in an appropriate solvent. The reduction potential of the oxophilic metals is much more negative than that of platinum, and simultaneous reduction of both metals is required for the formation of homogeneous particles with uniform composition. A necessary (but not sufficient) condition for the preparation of homogeneous nanoparticles is the use of very strong reducing agents, so that the electron transfer rate to all relevant metals is high compared to the mixing and diffusion rates of the reducing agent. Further, many of the metals of interest are very susceptible to oxidation, and strict air-free handling techniques need to be used until the final product is formed. This precaution is needed for every step from synthesis to washing and annealing the product. Any air introduced into the system may react with the particle surface and partially or completely oxidize the metal(s), resulting in nanoparticles that are mixed metal and oxide phases. The wash solvents have also been found to be of great importance since certain solvents, like alcohols and water, have been found to react with and dissolve (leach) the secondary oxophilic metal out of the nanoparticles resulting in uncontrolled surface stoichiometries and/or even pure Pt particles.[9,22]

Synthesis of these intermetallic phases as nanoparticles may require annealing either in the mother liquor or post synthesis. If the target composition has a high melting point, the associated very low diffusion rates at room temperature may necessitate heating to allow nucleation or ordering of the intermetallic phase. In our previous work, we have demonstrated the ability to successfully synthesize intermetallic phases with dimensions in the nanoregime but have found that the high temperatures required to nucleate ordered phases will cause any organic residues that bind to the nanoparticle surface to decompose forming carbonaceous solids that coat the particle surfaces, rendering them catalytically inactive.[22] These organic residues can be present in the precursors as ligands or anions, in the reducing agent, or even be bound or decomposed solvent molecules. In order to understand the role of such residues in limiting or inhibiting the preparation of active nanoparticles, the preparation of a specific intermetallic phase, PtNi, was studied using different reducing agents and metallic precursors to determine the source of this surface contamination and methods to optimize the activity of the resulting intermetallic nanoparticles.

PtNi was chosen since it is known to be catalytically active for fuel cell reactions including methanol oxidation and oxygen reduction.[23−28] Additionally, PtNi is important for several other catalytic reactions including hydrogenation and reforming reactions, all of which would require pristine surfaces to maximize the catalytic activity.[29−32] Further, nickel is moderately oxophilic so air-free synthesis and handling techniques can be simultaneously developed to avoid significant oxidation of the Ni. PtNi alloys have been synthesized previously using a variety of methods including hydrothermal, microwave irradiation, hydrazine, borohydride, and hydrogen reductions.[23,24,29,33,34] These synthetic methods, which are primarily aqueous, are effective for preparing solid solutions or alloys of the metals but do not result in the atomically ordered phase and cannot be adapted to oxophilic metals with very negative reducing potentials. To generate a more materials general synthesis route to intermetallic nanoparticles, we have developed an air-free synthesis technique which incorporates strong reducing agents and allows access to PtNi intermetallic nanoparticles with catalytically active surfaces. Through this case study, a new metal precursor, Li_2NiCl_4, that has not previously been used for the synthesis of metal nanoparticles, was also developed. Unlike many transition metal binary chlorides, this precursor is quite soluble in organic solvents like THF, which eliminates the organic ligands from the metal precursors in the reaction. Since PtNi is catalytically active, this activity can be used as a probe to determine the effect of each modification to the synthesis and optimize the reaction for the best activity. For this study, formic acid oxidation was used as a probe of catalytic activity because it typically produces CO during the reaction, so CO poisoning can also be investigated. This is the first investigation of activity for formic acid oxidation by PtNi that has been reported.

EXPERIMENTAL SECTION

The following materials were used as purchased from STREM Chemicals Inc.: platinum(II) 2,4-pentanedionate ($Pt(acac)_2$), dichloroplatinum cyclooctadiene ($Pt(COD)Cl_2$), nickel(II) 2,4-pentanedionate ($Ni(acac)_2$), nickel chloride $NiCl_2$, lithium chloride, and sodium metal. Naphthalene, potassium triethylborohydride $KBH(Et)_3$, lithium triethylborohydride $LiBH(Et)_3$, *n*-butyl lithium, THF, hexanes, and anhydrous methanol were purchased from Aldrich. THF and hexanes were dispensed from a custom built Seca solvent system by Glass Contour.

Synthesis of PtNi Nanoparticles. For all reducing agents except sodium naphthalide, the reaction conditions were as follows: platinum and nickel precursors (0.25 mmol each) were weighed out in an argon filled glovebox and dissolved in 40 mL of THF by stirring. Then the reducing agent ($KBH(Et)_3$, $LiBH(Et)_3$, or *n*-BuLi) (10% excess) was drawn up into a syringe and injected into the stirring Pt/Ni solution, which instantly (a few seconds at most) formed an opaque black solution. The solution was then stirred for 1−4 h and left standing to see if all the product(s) precipitate out. When the borohydride reducing agents are used, a dark precipitate would crash out almost immediately, but with *n*-BuLi no precipitate was observed. The products that completely precipitate were washed by decanting off the clear THF reaction solution and adding in fresh THF with stirring, reprecipitating the product, and again decanting the solution above the precipitate and repeating this wash three times. When *n*-BuLi is the reducing agent, the product does not precipitate out even after standing for more than 24 h. That solution was subsequently transferred to a centrifuge tube, sealed, and brought out of the box and centrifuged at 9000 rpm for 30 min. If the product did not come out of solution by centrifuging, the solvent was removed under vacuum and the product washed with hexanes, followed by hexanes and small amounts of THF. All products were then dried under vacuum and pumped into the glovebox. Samples that were annealed to form the intermetallic phase were placed into silica tubes in the glovebox and then brought out and sealed under vacuum without air exposure. All samples were annealed at 500 °C for 24 h unless otherwise mentioned.

Sodium Naphthalide. Sodium naphthalide solution was prepared in THF according to well-known literature methods.[35] Sodium metal (0.0349 g, 1.5 mmol) and naphthalene (0.2021, 1.5 mmol) were weighed out in an argon atmosphere glovebox and added to a flask with 40 mL of THF. The sealed flask was removed from the glovebox and stirred overnight under argon to produce a dark green sodium naphthalide solution.

A THF solution of platinum and nickel precursors (0.25 mmol each) was prepared in the glovebox, then sealed, brought out, and injected into the stirring sodium naphthalide solution. The dark green solution immediately turned black. The PtNi nanoparticle solution was stirred

for 3 h then worked up in the same manner as the above reactions including centrifuging and washing with THF and hexanes.

Characterization. Powder X-ray diffraction (pXRD; Scintag XDS 2000; Cu Kα radiation (λ = 0.15418 nm) was used for structural characterization. Thermogravimetric analysis was performed on a TA Instruments Q50 under flowing argon using aluminum pans, 5−10 mg of sample, and a heating rate of 10 °C min^{-1}. Images were taken on a scanning electron microscope (SEM; LEO-1550 field emission SEM) with energy dispersive X-ray analysis (EDS), and on a transmission electron microscope (TEM; FEI Tecnai G2 T12 Spirit) with selected area electron diffraction (SAED). Isopropyl alcohol suspensions of the samples were dispersed on Si wafers for SEM observation and on commercial copper grids for TEM, respectively. The surface area of the samples was measured using a Micromeritics ASAP 2020 to collect a partial adsorption isotherm at liquid nitrogen temperature (−196 °C) with krypton or nitrogen as the adsorption gas over the pressure range (P/P_0) of 0.06 and 0.5. The samples were degassed under vacuum at room temperature for 48 h prior to the measurement. The specific surface area was determined according to the Brunauer−Emmett−Teller (BET) method in the relative pressure (P/P_0) range of 0.08−0.185.

Electrocatalytic Activity. The electrocatalytic activity of the PtNi nanoparticles was tested for formic acid oxidation. Prior to each experiment, a suspension of the nanoparticle catalyst was prepared as follows: to 8 mg of the dried nanoparticle sample were added 3.98 mL of distilled water and 1 mL of isopropyl alcohol (Aldrich). Additionally, 20 μL of a 5% (w/w) Nafion solution in alcohols and water (Aldrich, EW: 1100) was added to this mixture. The resulting mixture was sonicated in a bath type ultrasonicator for 1 h. The nanoparticle suspension was then coated onto a 4 mm diameter glassy carbon (GC) electrode. The GC electrode had been previously polished with diamond paste (METADI-Buehler, ø = 1 μm) and ultrasonicated in Millipore water (18 MΩ cm^{-1}, Millipore Milli-Q) for 10 min. The electrode was then rinsed with Millipore water and allowed to dry in air. 140 μg cm^{-2} of the nanoparticle (10.8 μL of nanoparticle suspension) was coated onto the clean GC electrode. The coated electrode was then dried in air.

Formic acid oxidation on the nanoparticle-coated GC electrode was examined in a mixture of 0.5 M formic acid (Mallinckrodt, 88% analytical reagent) and 0.1 M sulfuric acid. A three-electrode electrochemical cell was used for all electrochemical measurements. The reference electrode was a sodium chloride saturated Ag/AgCl electrode, and the counter electrode was a platinum coil. All electrochemical experiments were carried out at room temperature with a Pine AFRDE2 potentiostat. All solutions were prepared with Millipore water and deaerated with prepurified argon for at least 15 min before each experiment.

RESULTS AND DISCUSSION

Synthesis Conditions and Reducing Agents. To keep as many parameters the same, all experiments were conducted under similar conditions using THF as the solvent and washing the products with THF and hexanes prior to annealing or air exposure to avoid partial oxidation of the Ni from other wash solvents like alcohols and water. The reaction in Scheme 1 shows the synthetic process for producing PtNi intermetallic nanoparticles.

The reduction of these metal precursors occurs very rapidly resulting in an instantaneous black colored solution for the individual metals and mixtures of both. As will be discussed in detail later, the particles made at room temperature were quite small (∼2−4 nm). Because of this, it is quite difficult to uniquely determine the atomic structure using standard diffraction techniques due to the broad diffraction peaks. To observe atomic ordering in these particles, the as-made samples were then sealed under vacuum in a silica tube and annealed at 500 °C for 24 h to increase the particle size. If the metals are not already crystallographically ordered, heating will promote particle growth as well as the formation of the ordered intermetallic phase. The samples were kept under inert atmosphere to minimize oxidation of Ni in air throughout each step of the synthesis and annealing. To avoid rapid oxidation and ignition of the nanoparticles after annealing, the samples were slowly exposed to air by piercing a septum on the argon filled sample container with a syringe needle, allowing the very slow in-diffusion of air and minimal surface oxidation. After 24 h, the container can be opened with no noticeable sintering or oxidation of the particles. At this point the product can be washed with water to remove any ionic byproducts.

Scheme 1

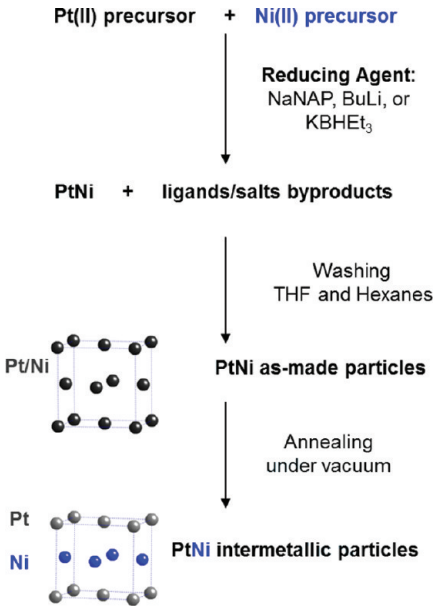

For this study, several different reducing agents were investigated including alkylborohydrides, butyl lithium (BuLi), and sodium naphthalide (NaNAP). The reducing agent needs to be strong enough to rapidly reduce the transition metals to avoid forming inhomogeneous products that result when very different metal reduction rates are obtained. Sodium naphthalide (NaNAP) is the strongest reducing agent utilized, while the reduction potential of *n*-BuLi is only about 0.5 V more positive.[36−38] BuLi was chosen since it is a strong reducing agent similar to sodium naphthalide but with very different leaving groups, as the butyl groups should form octane which can be easily washed away. Potassium triethylborohydride ($KBH(Et)_3$) was also used as a reducing agent due to its solubility in nonaqueous/ether solvents that are required for the other reducing agents. $KBH(Et)_3$ is not as strong as sodium naphthalide or butyl lithium but rapidly reduces both Pt and Ni and has soluble triethylboron byproducts that should not interfere with the surface of the resulting nanoparticles.

Synthesis of PtNi Using $Pt(acac)_2$ and $Ni(acac)_2$. Metal acetylacetonate (acac) precursors were initially selected due to their solubility in ethereal solvents which were required for the reducing agents. The reduction of these metal precursors, shown

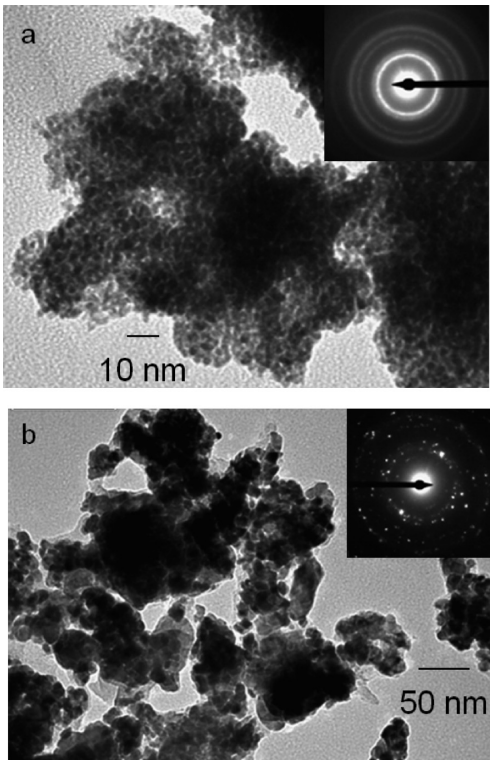

Figure 1. Transmission electron microscope (TEM) images of PtNi nanoparticles made with $Pt(acac)_2$ and $Ni(acac)_2$ using $KBH(Et)_3$. (a) The as-prepared particles are 2−3 nm in diameter, and (b) after annealing the sample at 500 °C nucleates the intermetallic phase as seen by the electron diffraction pattern inset in the images. Some aggregation and sintering occurs during annealing creating particles that are 15−20 nm in diameter.

below for a sodium naphthalide reduction, results in the instantaneous formation of a dark black solution.

$$Pt(acac)_2 + Ni(acac)_2 + 4Na\cdot naphthalene \rightarrow PtNi + 4Na(acac) + 4naphthalene$$

The resulting particles were then washed, dried, and annealed at 500 °C for 24 h to nucleate the intermetallic PtNi phase. After annealing, the silica annealing tubes were found to be coated on the inside with a black carbonaceous layer, no doubt from the decomposition of organic residues. Figure S1 (Supporting Information) shows the X-ray diffraction patterns confirming the formation of the intermetallic phase in the products after annealing at 500 °C.

To get a better idea of the particle sizes, transmission electron microscopy (TEM) was used to look at the particles and their crystallinity. The as-made particles were indeed very small (2−3 nm) as seen in Figure 1, and the electron diffraction patterns for these samples show diffuse rings similar to the broad X-ray diffraction patterns. Consequently, confirming the presence of the ordered intermetallic phase at this size regime is very difficult. After annealing these particles to 500 °C for 24 h, the particle size increases significantly, creating a much sharper diffraction pattern and producing spots in the electron diffraction image as seen in the inset of Figure 1b. The rings of diffraction spots index to that expected for the intermetallic phase PtNi confirming the XRD results of Figure S1 (Supporting Information).

Table 1. Particle size, Elemental Analysis, and Percent TGA Weight Loss of PtNi Nanoparticles Made with Different Reducing Agents and Metal Precursors

precursors	reducing agent	particle size (nm) as-made, 500 °C	% nickel	% wt loss
$Pt(acac)_2 + Ni(acac)_2$	NaNAP	~3, 18	55	36%
$Pt(acac)_2 + Ni(acac)_2$	$KBH(Et)_3$	~3, 14	61	21%
$Pt(acac)_2 + Ni(acac)_2$	*n*-BuLi	~3, 16	47	30%
$Pt(COD)Cl_2 + Li_2NiCl_4$	NaNAP	4, 21	53	6%
$Pt(COD)Cl_2 + Li_2NiCl_4$	$KBH(Et)_3$	4, 19	46	5%
$Pt(COD)Cl_2 + Li_2NiCl_4$	*n*-BuLi	3, 17	58	25%
$Li_2PtCl_6 + Li_2NiCl_4$	$KBH(Et)_3$	4, 18	45	6%
$Li_2PtCl_6 + Li_2NiCl_4$	$LiBH(Et)_3$	4, 19	47	9%

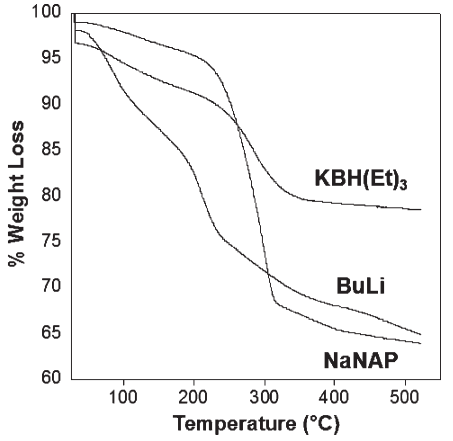

Figure 2. Thermogravimetric analysis (TGA) of PtNi nanoparticles made with $Pt(acac)_2$ and $Ni(acac)_2$ using $KBH(Et)_3$, sodium naphthalide (NaNAP), and *n*-BuLi. The percent weight losses for each synthesis method are 21, 36, and 35% respectively.

The composition of the particles was checked using energy dispersive X-ray spectroscopy (EDS) attached to the scanning electron microscope (SEM). The average composition for the products, taken from 5 to 8 different spots per sample, was found to be approximately 50:50 Pt:Ni ± 5% (see Table 1) based on the metal content and homogeneous throughout the sample for each of the different reducing agents. Atomically ordered PtNi exists over some composition range, from about 40−55% Pt at 400 °C in the bulk phase diagram,[39] so some variation in the composition of individual nanoparticles may occur. While the carbon composition is more difficult to accurately determine using this technique, significant carbon content was detected for all acac products, both as-made and annealed, that was much higher than a neighboring clean spot on the silicon sample holder. This implies that there is still a significant amount of carbon present on the surface or even in the bulk of the particles.

The thermogravimetric data for the different reducing agents showed that all of the as made products had significant weight loss due to the volatilization of organic decomposition products as seen in Figure 2. The samples were all heated at a rate of 10 °C/min under flowing argon to prevent oxidation of the particles and thus giving access to weight loss information about the volatilization of side products. The percent weight loss for materials prepared by the sodium naphthalide and *n*-BuLi synthesis is very similar. The lowest weight loss came from the

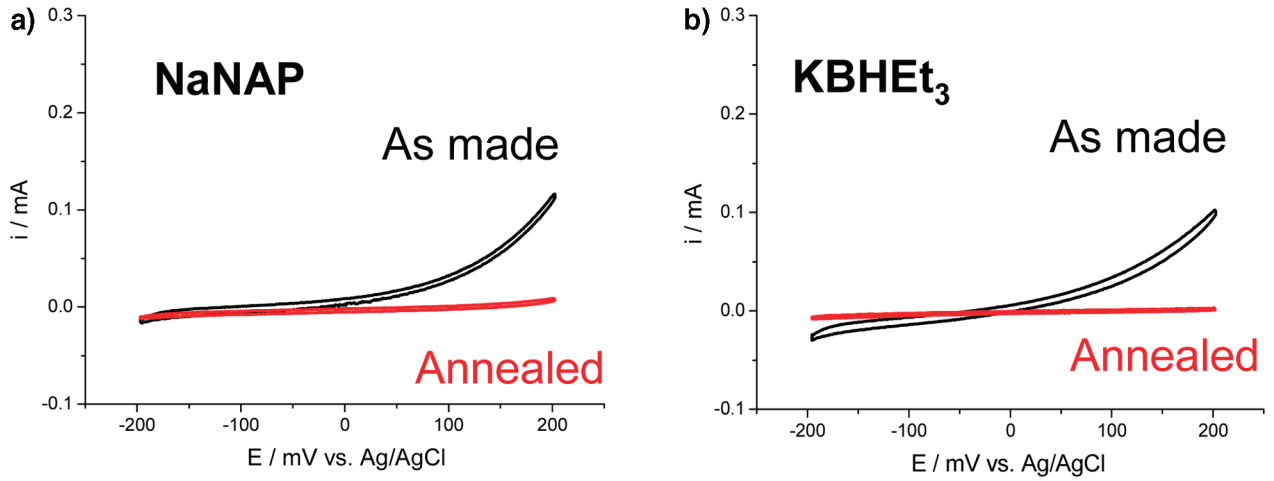

Figure 3. Cyclic voltammetry of PtNi nanoparticles made with $Pt(acac)_2$ and $Ni(acac)_2$ precursors using (a) sodium naphthalide and (b) $KBH(Et)_3$. The black scans are from as-made particles and the red scans are from the same sample after heating to 500 °C for 24 h.

$KBH(Et)_3$ synthesis, but there is still a large amount of trapped organic residue in the as-prepared products. The residue certainly resides on the surface of the particles but might also be trapped within the particles. Residue on the surface could potentially block or poison the surface of the catalyst particles. The borohydride reducing agent was expected to have the lowest amount of weight loss because the trialkylboron leaving group should only coordinate weakly with the surface of the metal nanoparticles and should be removed by the THF wash. In contrast, naphthalene is known to strongly bind to the surface of Pt metal and thus would be expected to have much greater amount of residue left behind after the synthesis.[40] BuLi was expected to have a smaller amount of weight loss because the butyl groups will likely combine and form octane as a product which would be easily washed away. However, BuLi also forms some sort of reactive complex in THF that eventually results in polymerization of the THF. It could be the species produced in this reaction also bind to the surface of the particles. Since all of these products did have a significant weight loss, it was concluded that the acetylacetonate (acac) ligand was a principle source of the organic residue.

To help elucidate the source of the surface contamination, the product was characterized with IR spectroscopy looking for the C−O stretch of the acac ligand which should appear around 1600 cm^{-1}, but no observable peaks were seen in this region. This may be due to the high absorption expected for the metal nanoparticles or different surface binding modes broadening the C−O band, or the ligand itself has been chemically altered or decomposed by the strong reducing agent or by the catalyst.

The electrocatalytic analysis of these particles is another characterization tool, since it will give insight into whether the surface is clean and active or inactive due to organic or carbonaceous coatings (poisons). Formic acid oxidation was chosen for this analysis because it will give information about the activity of the catalytic particles as well as insights about poisoning by CO because CO is an intermediate of the reaction.[41] Formic acid oxidation on platinum is thought to occur through a two-step mechanism producing CO_2, H^+, and electrons.

$$HCOOH + Pt \rightarrow Pt-(COOH) + H^+ + e^-$$

$$Pt-(COOH) \rightarrow Pt + CO_2 + H^+ + e^-$$

The second reaction occurs through a reactive intermediate that can give rise to CO as a side product.

The samples were cycled between −0.2 and 0.2 V to determine the onset potential of formic acid oxidation and the amount of current produced by this reaction. Above 0.2 V, there was evidence of Ni leaching from the catalysts; consequently all testing was performed below this value. As expected due to the formation of carbonaceous deposits, the small amount of activity seen in the as-made PtNi samples was lost upon annealing as seen in Figure 3. The annealed BuLi samples were also not catalytically active. At this point, it was clear that BuLi is not an optimal reducing agent for reactions in THF, due to side reactions of the BuLi with THF.

The electrocatalytic activity of these samples did contain some useful information about the coating on the particles. The as-made samples have organic species present as seen by TGA and produce a carbon deposit on the silica tubes used for annealing, but initially this species is not bound tightly enough or at sufficient density to block all catalysis on the surface. Once these particles are annealed, however, the surface bound species decomposes forming a carbonaceous coating that completely blocks the catalytic sites, making the particles totally inactive. To confirm this hypothesis, Raman spectroscopy was used to look for carbon in the annealed products. Two sharp peaks were found at 1580 cm^{-1} and 1350 cm^{-1}, which are known to be the ordered (E_{2g}) and disordered (A_{1g}) graphite peaks, respectively.[42]

In the as-made sample produced by sodium naphthalide reduction, there is no evidence in the IR of naphthalene present in the sample. A significant amount of sodium is detected by EDS, which implies that there is a negatively charged species present on the surface requiring a counterion (Na^+) to balance the charge. This makes sense if the acac ligand is still bound but there is no other direct evidence for the presence of acac. There are no other hints about what this surface bound species is and the weight loss in TGA occurs over a broad range of temperatures and is different for each reducing agent. Therefore, most of the organic species were eliminated from the reaction to reduce the possibility of forming this carbonaceous shell on the particles

Synthesis of PtNi Using Chlorine Based Precursors. In order to eliminate the organic species present, chloride based metal precursors were sought. However, nickel chloride ($NiCl_2$) is not soluble in THF, so another nickel chloride compound was

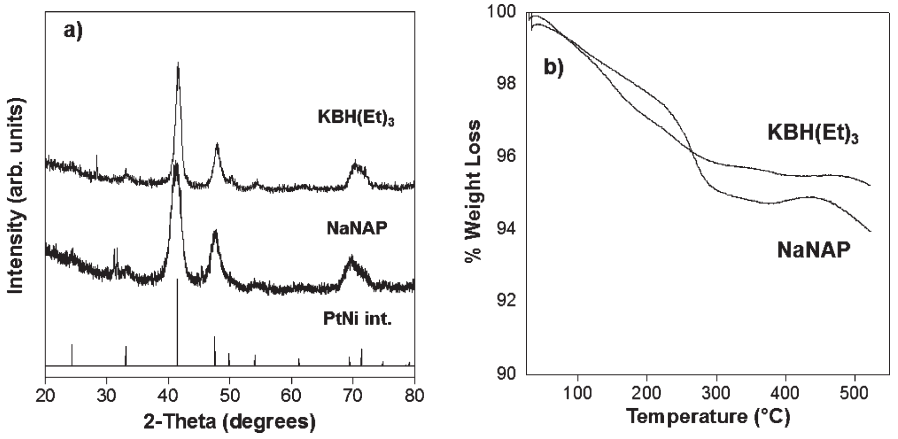

Figure 4. (a) XRD patterns of PtNi nanoparticles annealed at 500 °C made with Li_2NiCl_4 and $Pt(COD)Cl_2$ precursors using $KBH(Et)_3$ and sodium naphthalide (NaNAP). The peak positions for the intermetallic phase of PtNi (PDF # 30652797) are shown as tick marks at the bottom. All the ordering peaks are expected to be weak, as observed. (b) Thermogravimetric analysis (TGA) of PtNi nanoparticles made with Li_2NiCl_4 and $Pt(COD)Cl_2$ using $KBH(Et)_3$ and sodium naphthalide. The percent weight losses for each synthesis method are 5 and 6, respectively.

needed that could be easily made and is soluble in ether solvents. Li_2NiCl_4 has been studied spectroscopically in several molten salts, and it was hypothesized that the polarizing power of the small Li^+ ion would help pull the tetrahedral $NiCl_4^{2-}$ ions into solution.[43−45] Li_2NiCl_4 was synthesized according to the phase diagram by heating LiCl and $NiCl_2$ in a sealed silica tube for 7 days at 580 °C followed by quenching to room temperature in water. The crystal structure of Li_2NiCl_4 has not been reported, perhaps due to its sensitivity to air and/or water. However, the Li_2NiCl_4 can be readily dissolved in THF resulting in a bright blue solution, whereas $NiCl_2$ is quite insoluble in THF and forms only an orange suspension.

A solution of this salt (Li_2NiCl_4) with $Pt(COD)Cl_2$ (COD = cyclooctadiene) was then reduced with sodium naphthalide (NaNAP) or potassium alkylborohydride as shown below.

$$Pt(COD)Cl_2 + Li_2NiCl_4 + 4KBH(Et)_3 \rightarrow PtNi + 2LiCl + 4KCl + COD + 4B(Et)_3 + 2H_2$$

All organic species (COD, naphthalene, alkylboron, and THF) remaining after reaction are expected to be neutral. The same synthesis, washing procedures, and reducing agents were used to compare the chlorine based precursors to the data collected for the acac precursors.

The XRD of the as-made particles have an fcc alloy type pattern that is shifted to higher angles than for the pure platinum positions (between those expected for Pt and Ni indicating some degree of alloying as seen in the Supporting Information (Figure S2). Additionally, when Li_2NiCl_4 is reduced by itself to form Ni nanoparticles, they are all quickly attracted to the magnetic stir bar, whereas the PtNi sample simply precipitates to the bottom with no interaction with the stir bar providing further evidence that the particles are alloyed. All the as-made samples from the chloride precursors had a more defined XRD pattern than that observed from the acac precursors indicating that the crystal domains are larger and more crystalline. The Scherrer equation could not be applied to the acac samples because of weak intensity and very broad peaks. For the chloride based precursors, however, the Scherrer equation indicates 4 nm domain sizes for the sodium naphthalide and potassium borohydride reductions.

Additionally, the precipitation behavior is also noticeably different for the chloride based precursors. The as-prepared PtNi particles precipitated out of solution within minutes after reduction leaving a clear colorless solution. This is very advantageous because LiCl is soluble in THF and thus most if not all of the LiCl byproduct can be simply washed away with THF. Presumably these particles precipitate because any species bound to the surface do not prevent agglomeration.

It is clear from TGA data that these products contain significantly less or no organic species with weight losses at 5 and 6% for $KBH(Et)_3$ and NaNAP, respectively. The NaNAP sample shows a small weight increase (0.5%) at 400 °C that is likely due to an oxygen contamination coming from the argon gas. The products formed during the TGA experiments showed the intermetallic PtNi phase by XRD so this oxidation is relatively minor. The particles made with chloride precursors probably have some chlorine bound to the surface which will be counter balanced with cations in solution, and electrochemical studies show that that Cl^- binds to Pt and many other metal surfaces.[46,47] Since Li^+ interacts strongly with THF and NaCl and KCl are so insoluble, it is possible that either the K^+ or the Na^+ ions associate with the Cl^- bound to the surface and aid in aggregation and precipitation. Additionally, these insoluble salt side products may serve as nucleation sites for the aggregation of PtNi particles and help to precipitate them out which will be discussed in detail later.

The as-made samples were then sealed under vacuum in a silica tube and annealed to form the intermetallic phase. After annealing the samples at 500 °C for 24 h, the samples were manipulated in an inert atmosphere glovebox to minimize oxidation of Ni in air and were slowly exposed to air as previously described for characterization. Interestingly, annealing the NaNAP and $KBH(Et)_3$ products did not result in any visible carbonaceous deposits. Figure 4 shows the XRD patterns in which the ordering peaks are present providing evidence that the intermetallic phase has formed. It also appears like the NaCl preferentially binds to the particles blocking the adsorption of naphthalene molecules at the surface since the larger weight loss seen in TGA usually associated with the use of naphthalene is not observed and there is not a carbonaceous deposit on the annealing tube.

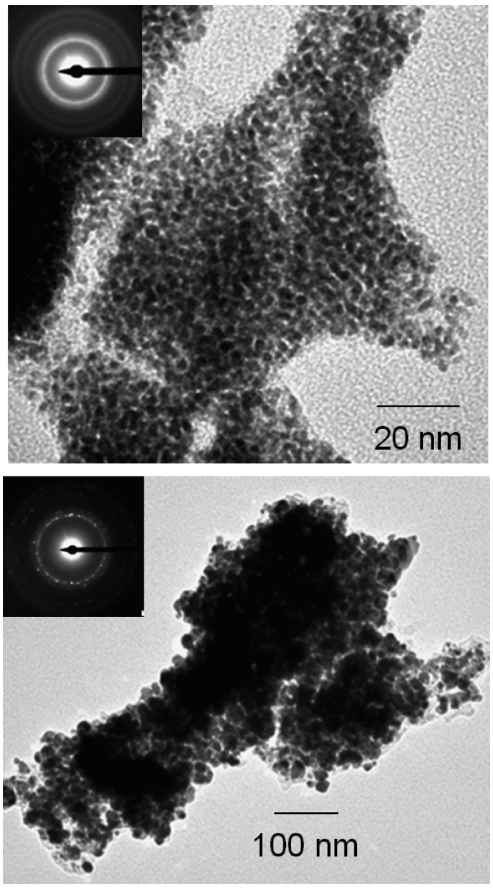

Figure 5. Transmission electron microscope images of PtNi nanoparticles made with Li_2NiCl_4 and $Pt(COD)Cl_2$ precursors using $KBH(Et)_3$. (A) As-prepared the particles are 2−3 nm in diameter, and (B) annealing the sample at 500 °C nucleates the intermetallic phase as seen by the electron diffraction pattern inset in the images. Some aggregation occurs during annealing, creating particles that are 15−20 nm in diameter.

The samples were examined before and after washing them with water to remove any salts (KCl and NaCl), and no noticeable differences in the metal particles were observed by XRD, TEM, or EDS. The surface of these particles no doubt partially oxidizes in air, but the intermetallic phase is maintained proving that the bulk of the samples remains unchanged. The particle size of the annealed products does vary slightly with reducing agent from 17 to 21 nm in size, but no clear correlation can be drawn about the particle size and reducing agent. The precursors do seem to have an effect, however, as the chlorides are generally larger and more crystalline products.

TEM imaging of the particle size obtained from the chloride precursors looked similar to those prepared with the acac precursors in dimension, but with less visible "coronas" on the latter particles that presumably arise from organic residues, as seen in Figure 5. The as-made particles are 3−4 nm in diameter and have diffuse fcc type diffraction patterns indicating that they are alloyed but still too small to see ordering peaks indicative of the intermetallic phase. The annealed sample shows well faceted particles that are around 20 nm in size that have a very crystalline diffraction pattern matching that of the ordered phase. The range of particle sizes is to be expected since there was no attempt to control the sintering and no surface stabilizing agents are present. All the samples made from Cl precursors have very little low density coatings, consistent with a significant reduction of light elements or organic materials on the particle surfaces.

Additionally, EDS data from the SEM analysis indicate that there is little C present in the chloride samples ($\leq$5%) but a significant amount (~40%) present in the acac samples. These samples were supported on a silicon wafer to reduce the amount of C detected from the support, but the results are still not quantitative since the Si wafer was not meticulously cleaned before loading the samples. Nonetheless, there is a very noticeable difference in products from the acac and chloride precursors. Additionally, after washing with water (to remove all KCl and NaCl), the amount of chlorine seen by EDS was below the detectable limits of the instrument. This does not mean that the surface of the particles is completely free of chlorine. For 15 nm nanoparticles, if every metal atom at the surface were bound to Cl, then the mole fraction of Cl would be about 12% and that amount would be easily detected. If the surface coverage was a factor of 10 or more lower, the chlorine signal would be difficult to detect above background noise. The average composition obtained by EDS for Pt:Ni made with Cl precursors was typically 50:50 ($\pm$3%) and uniform throughout the sample. The composition and particle sizes are all compiled in Table 1 to compare the different reducing agents and precursors.

Electrochemical measurements were used to determine the activity of the particles by investigating accessibility of exposed electroactive metal sites. The difference between acac and Cl^- precursors is immediately apparent. The as-made samples show similar activity to the acac precursors but there does not seem to be any trend to the activity obtained with different reducing agents at this point. However, a significant difference is observed when comparing the annealed samples. For the acac precursors, none of the annealed samples showed any activity, but for the Cl precursors, a dramatic enhancement in activity is observed upon annealing (Figure 6).

This increase occurs even though the particle size increases significantly, as observed by XRD and TEM, leading to a decrease in surface area, but the activity is still significantly higher than that of the unannealed samples. It was assumed that this increase in activity is due to the atomic ordering of the metals within the sample providing a more active surface for the oxidation of formic acid. The activity per unit surface area of these samples increases as much as an order of magnitude upon annealing. The activity of the $KBH(Et)_3$ sample was much higher than that of the NaNAP sample even though their composition and percent weight loss is similar. The reason for this difference is under further investigation, but may be due to the inclusion of boron since nickel is known to incorporate boron when reduced with borohydride species under certain conditions.[48]

Because the annealed samples showed greatly improved electrocatalytic activity, lower temperature annealing was also probed. A large batch of the most active phase was synthesized using $KBH(Et)_3$, $Pt(COD)Cl_2$, and Li_2NiCl_4 precursors and annealed portions of the product at several different temperatures. XRD clearly shows the appearance of ordering peaks by 500 °C, as well as the expected shifts in the main diffraction peaks coming from the changes in unit cell parameters on ordering as seen in Figure 7.

The diffraction peaks shift toward the positions expected for the bulk alloy phase on heating up to 300 °C, and then at 500 °C the ordering peaks are visible. By 600 °C, the pattern looks much more crystalline with even larger domain sizes, but the line

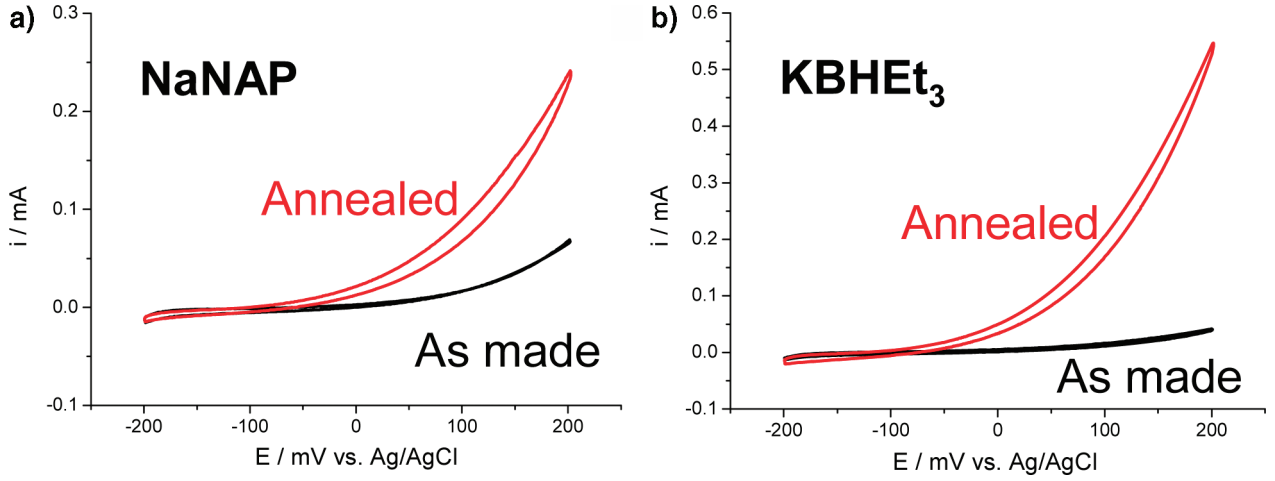

Figure 6. Cyclic voltammetry of PtNi nanoparticles made with Li_2NiCl_4 and $Pt(COD)Cl_2$ precursors using (a) sodium naphthalide and (b) $KBH(Et)_3$. The black scans are from the particles as-made, and the red scans are from the same sample after heating to 500 °C for 24 h.

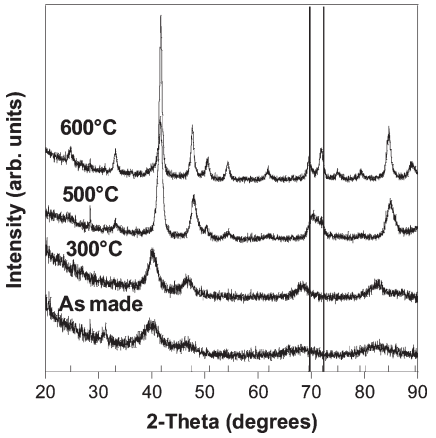

Figure 7. XRD patterns of PtNi nanoparticles made with Li_2NiCl_4 and $Pt(COD)Cl_2$ precursors using $KBH(Et)_3$ (a) as-made and heated to (b) 300, (c) 500, and (d) 600 °C. The peak positions for the intermetallic phase of PtNi (PDF # 30652797) are shown as tick marks at the bottom with two lines added to highlight the change in peak positions on going from alloy to intermetallic.

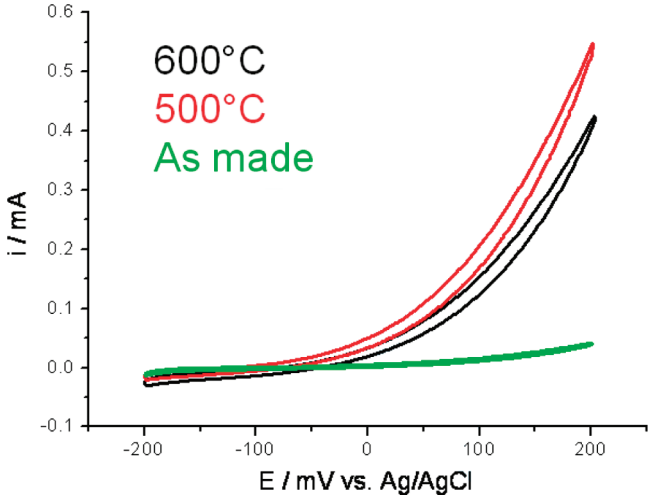

Figure 8. Cyclic voltammetry of PtNi nanoparticles made with Li_2NiCl_4 and $Pt(COD)Cl_2$ precursors using $KBH(Et)_3$. The green scan is from the particles as-made, and the red and black scans are from the same sample after heating to 500 and 600 °C for 24 h, respectively. A sample was also heated to 300 °C, but it directly overlapped the as-made sample and was removed for clarity.

positions are not shifted from the 500 °C sample. This means that the intermetallic phase has formed at 500 °C; heating to 600 °C only increases the particle size. The electrocatalytic activity of these samples shows a similar behavior as that seen in Figure 8.

The as-made sample and the 300 °C sample both have very similar activities (300 °C not shown for clarity), and the 500 and 600 °C samples show greatly enhanced activity. This increase in activity appears to be a result of the atomic ordering that occurs upon annealing at higher temperatures. The activity of the 600 °C sample is slightly lower than that of the 500 °C sample, likely due to the smaller surface area of the former product. The particle size as determined by the Scherrer equation gives 16 nm for the 500 and 19 nm for the 600 °C sample, respectively. While the Scherrer equation is only an estimate of the average domain sizes, the surface area of the 600 °C sample is decreased compared to the 500 °C samples but more than the catalytic activity suggests. Thus there may be more complicated surface phenomenon at work here but our working hypothesis is that the difference in activity mostly coordinates with the differences in surface area.

Because the annealed samples from the Cl precursors showed enhanced activity, the remaining organic ligand (COD) was eliminated from the reaction in an attempt to further optimize the catalytic activity and onset potential. An organic free Pt precursor, Li_2PtCl_6, was synthesized by a simple reaction of H_2PtCl_6 and Li_2CO_3 in water followed by removing the waters of hydration through heating under vacuum at 180 °C. By using only Li_xMCl_y precursors, the reaction byproducts are greatly simplified and the number of different species present to bind with the surface of the catalyst is decreased. A solution containing a 1:1 molar ratio of Li_2PtCl_6 and Li_2NiCl_4 was reduced using $KBH(Et)_3$ as the reducing agent.

$$Li_2PtCl_6 + Li_2NiCl_4 + 6KBH(Et)_3 \rightarrow PtNi + 4LiCl + 6KCl + 6B(Et)_3 + 3H_2$$

Again the solution immediately turned black on addition of the reducing agent, and complete precipitation occurred in less than

dx.doi.org/10.1021/cm1024876 |*Chem. Mater.* 2011, 23, 1136–1146

5 min. The electrochemical data revealed a further enhancement in catalytic activity. This enhancement is thought to be due to the decrease in organic materials binding to the surface since COD and naphthalene are not present. While COD does not appear to adhere strongly enough to the as-made Pt−Ni surface to completely block catalytic activity (binding energy of cyclooctadiene (COD) to a Pt surface is about 20 kcal/mol), removing it from the reactants appears to have increased the catalytic activity, supporting the hypothesis that organic ligands and anions should be avoided for optimal catalytic activity.[49]

Next, the amount of insoluble salt side products was reduced by changing the reducing agent to $LiBH(Et)_3$ from $KBH(Et)_3$.

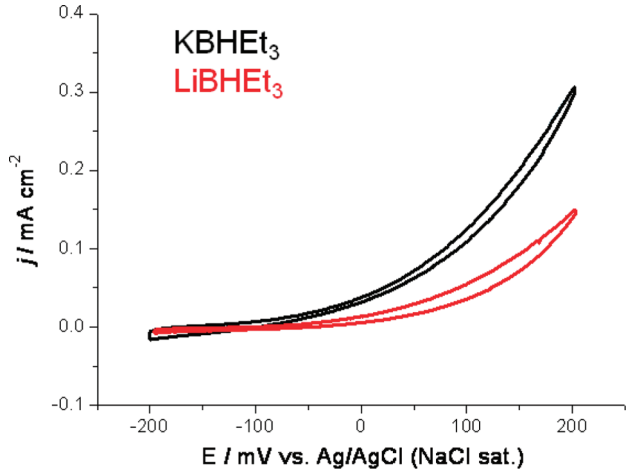

Figure 9. Cyclic voltammetry of PtNi nanoparticles made with Li_2NiCl_4 and Li_2PtCl_6 precursors using $LiBH(Et)_3$ and $KBH(Et)_3$ reducing agents and annealed at 500 °C for 24 h.

Table 2. Onset Potentials and Current Densities at Different Voltages for PtNi Nanoparticles for Formic Acid Oxidation (all specified potentials are vs Ag/AgCl (NaCl sat.))

		current density (m A cm^{-2})			
catalyst	onset potential (mV)	−100 mV	0 mV	+100 mV	+200 mV
$KBHEt_3$ 500	−170	0.007	0.037	0.125	0.305
$LiBHEt_3$ 500	−85	0	0.013	0.055	0.148

Thus the only salt byproduct is LiCl, which is soluble in THF and could be simply washed away without using any oxidizing solvents such as alcohols or water as is needed for NaCl or KCl.

$$Li_2PtCl_6 + Li_2NiCl_4 + 6LiBH(Et)_3 \rightarrow PtNi + 10LiCl + 6B(Et)_3 + 3H_2$$

The product still precipitated out of solution within 60 min. The supernatant was decanted off, and the remaining product washed several times with THF by stirring, reprecipitating, and decanting the supernatant. All these steps were carried out in the glovebox, with minimal exposure to trace oxygen and water (in the ppm range). The XRD from this sample had no observable salts in the as-prepared product and showed the typical fcc type alloy XRD pattern. These particles were then annealed under vacuum at 500 °C without exposure to air and formed very crystalline PtNi intermetallic particles with an average particle size of 18 nm. EDS analysis of this sample showed no observable Cl and a very low C content ~3%. The Pt:Ni ratio was 53:47 (± 5%, averaged over 5−1 μm^2 areas) which is very similar to the other samples discussed in this paper (Figure 9 and Table 2).

Electrocatalytic activity for this sample looked similar to that of the as-prepared sample, but the annealed sample showed a slightly reduced activity compared to the sample made with $KBH(Et)_3$. While the XRD pattern for the annealed sample shows phase pure PtNi intermetallic with domain sizes similar to those of the $KBH(Et)_3$ sample and the TGA shows a relatively small weight loss, the sample is less active. A closer investigation by TEM analysis reveals that there is a significant difference in the actual particle size (Figure 10).

The sample made with $KBH(Et)_3$ shows much smaller particles with less aggregation while the sample made with $LiBH(Et)_3$ shows an interconnected network of particles. This was expected since the sample made with $KBH(Et)_3$ forms KCl which is insoluble and either traps the resulting PtNi nanoparticles or provides a support limiting the aggregation. A TEM image of the unwashed KCl/PtNi sample is shown in the Supporting Information (Figure S3). The samples made with $LiBH(Et)_3$ only form LiCl, which is soluble in THF, and thus insoluble salts on the particle surface could not inhibit the growth and aggregation of the particles, as does KCl. Additionally, KCl was found to suppress the growth of the nanoparticles and increase the intermetallic formation temperature. The samples made with $KBH(Et)_3$ show intermetallic peaks only after annealing at 500 °C for 24 h while the sample made with $LiBH(Et)_3$

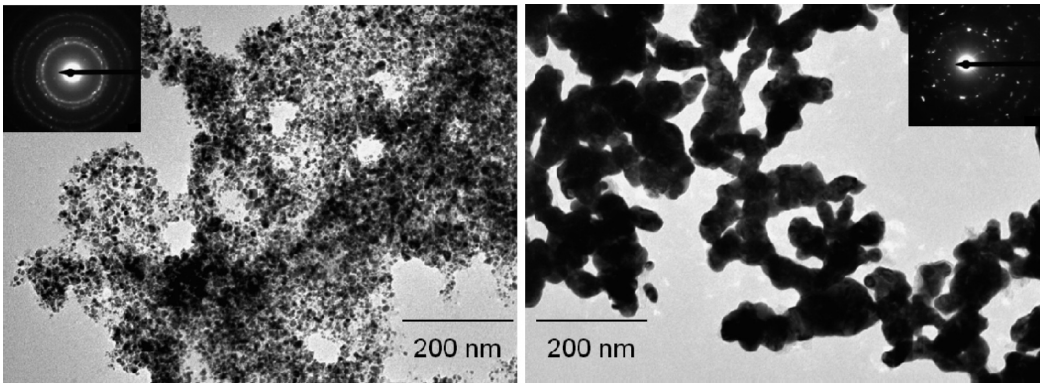

Figure 10. Transmission electron microscope (TEM) images of PtNi nanoparticles made with (a) $KBH(Et)_3$ and (b) $LiBH(Et)_3$ then annealed at 500 °C for 24 h. A greater degree of aggregation and sintering can be seen in the $LiBH(Et)_3$ sample than the $KBH(Et)_3$ sample due to the lack of KCl salt acting as a support during the annealing process.

forms the ordered phase by 400 °C. This difference in ordering temperature is thought to be due to the KCl limiting interparticle diffusion of Pt and Ni, thus inhibiting particle growth and possibly the nucleation of the ordered phase. Both of these outcomes may be useful in different circumstances. Since the primary interest of this investigation is the synthesis and catalytic activity of the intermetallic phases, using $LiBH(Et)_3$ as the reducing agent currently appears to inhibit particle growth and atomic ordering the least. The $KBH(Et)_3$ synthesis is useful for forming particles with higher surface area and literally creates a KCl support or encapsulant for these particles during the annealing stage, thus limiting the particle growth and aggregation. The sodium naphthalide reaction also forms an insoluble NaCl salt, which allows access to a stronger reducing agent and smaller particle sizes. Additionally, it appears that the NaCl prevents naphthalene from binding to the surface, keeping the particles free from carbonaceous deposits that can block the surface and limit catalytic activity. Depending on the desired nanoparticle characteristics, the two borohydrides and sodium naphthalide are useful reducing reagents for the formation of very small (3−4 nm) bimetallic particles with relatively clean surfaces, but some attention needs to be paid to the resulting byproduct salts and their affect on intermetallic formation temperature and resulting particles sizes.

CONCLUSIONS

The air-free synthesis of PtNi intermetallic nanoparticles was presented using a variety of reducing agents and metallic precursors. Through these studies, it was found that all the species present in the reaction solution can have an impact on the formation and composition of the nanoparticles and their catalytic activity. Post reduction removal of side products and thermal processing also has a great impact on the kinetics of formation of alloy or ordered phases and on their catalytic activity. It was shown that the use of metal acac precursors has a significant impact on the composition of the product because of the strong affinity of the anionic acac ligand with the surface of the metal particles. In an effort to avoid organic residues, a new chloride based precursor, Li_2NiCl_4, was developed which is soluble in ether solvents unlike many metal chlorides including $NiCl_2$. When using metal chloride precursors, a considerably lower weight loss was observed by TGA (5% compared to ∼30% for acac) indicating a smaller amount of organic material present. The remaining weight loss is likely due to adsorbed water and other species that accumulate on the sample in air while loading the samples into the TGA. The removal of bound surface species has several effects on the properties of the resulting particles including more rapid and complete precipitation behavior, which aids in cleaning up the product, and lower intermetallic formation temperatures. The intermetallic formation temperature is lowest when $LiBH(Et)_3$ is the reducing agent and metal chloride salts are used as the reactants. Additionally, the use of lithium metal chloride based precursors has led to much cleaner particle surfaces with greatly enhanced catalytic activity which allows the synthesis and study of intermetallic particles for fuel cell reactions. Several other Li_xMCl_y precursors have been synthesized and are currently being studied in an effort to extend this method to other Pt−M intermetallics. Because Ni is oxophilic, it is believed that the results presented here will transfer over to other more electropositive metals and lead to a generalized method for synthesizing and testing electrocatalytic activity of intermetallic nanoparticles. Combining this with nonpolar solvents and air-free conditions, this technique provides opportunity for the synthesis and testing of many intermetallic phases that may contain very electropositive metals.

ASSOCIATED CONTENT

Supporting Information. XRD, TEM, and onset potentials and current densities (PDF). This material is available free of charge via the Internet at http://pubs.acs.org.

AUTHOR INFORMATION

Corresponding Author

*Fax: 607-255-4137 Phone: (607) 255-7238. E-mail: fjd3@cornell.

ACKNOWLEDGMENT

This work was supported by the Basic Energy Sciences Division of the Department of Energy. The authors wish to thank Mick Thomas for help with the SEM data acquisition and analysis and John Grazul with the TEM. All of these tools are managed and maintained by the Cornell Center for Materials Research (CCMR), an NSF supported MRSEC through Grant DMR-0520404.

REFERENCES

(1) O'Hayre, R., Cha, S.-W.; Colella, W., Prinz, F. B. *Fuel Cell Fundamentals*; John Wiley and Sons: Hoboken, NJ, 2006.

(2) Lamy, C. L.; Leger, J. M.; Srinivasan, S. *Direct Methanol Fuel Cells: From a Twentieth Century Electrochemist's Dream to a Twenty-first Century Emerging Technology*, 2001.

(3) Gasteiger, H. A.; Gu, W.; Litteer, B.; Makharia, R.; Brady, B.; Budnski, M.; Thompson, E.; Wagner, F. T.; Yan, S. G.; Yu, P. T. In *Mini-Micro Fuel Cells: Fundamentals and Applications*; Kakac, S., Pramuanjaroenkij, A., Vasiliev, L., Eds.; Springer: New York, 2008; pp 225−233.

(4) Gasteiger, H. A.; Kocha, S. S.; Sompalli, B.; Wagner, F. T. *Appl. Catal., B* **2005**, *56*, 9–35.

(5) Long, J. W.; Stroud, R. M.; Swider-Lyons, K. E.; Rolison, D. R. *J. Phys. Chem. B* **2000**, *104*, 9772–9776.

(6) Yano, H.; Kataoka, M.; Yamashita, H.; Uchida, H.; Watanabe, M. *Langmuir* **2007**, *23*, 6438–6445.

(7) Wakabayashi, N.; Takeichi, M.; Uchida, H.; Watanabe, M. *J. Phys. Chem. B* **2005**, *109*, 5836–5841.

(8) Matsumoto, F.; Roychowdhury, C.; DiSalvo, F. J.; Abruña, H. D. *J. Electrochem. Soc.* **2008**, *155*, B148–B154.

(9) Abe, H.; Matsumoto, F.; Alden, L. R.; Warren, S. C.; Abruña, H. D.; DiSalvo, F. J. *J. Am. Chem. Soc.* **2008**, *130*, 5452–5458.

(10) Roychowdhury, C.; Matsumoto, F.; Zeldovich, V. B.; Warren, S. C.; Mutolo, P. F.; Ballesteros, M.; Wiesner, U.; Abruña, H. D.; DiSalvo, F. J. *Chem. Mater.* **2006**, *18*, 3365–3372.

(11) Alden, L. R.; Roychowdhury, C.; Matsumoto, F.; Han, D. K.; Zeldovich, V. B.; Abruña, H. D.; DiSalvo, F. J. *Langmuir* **2006**, *22*, 10465–10471.

(12) Alden, L. R.; Han, D. K.; Matsumoto, F.; Abruña, H. D.; DiSalvo, F. J. *Chem. Mater.* **2006**, *18*, 5591–5596.

(13) Roychowdhury, C.; Matsumoto, F.; Mutolo, P. F.; Abruña, H. D.; DiSalvo, F. J. *Chem. Mater.* **2005**, *17*, 5871–5876.

(14) Ranjan, C.; Hoffmann, R.; DiSalvo, F. J.; Abruña, H. D. *J. Phys. Chem. C* **2007**, *111*, 17357–17369.

(15) Casado-Rivera, E.; Volpe, D. J.; Alden, L.; Lind, C.; Downie, C.; Vazquez-Alvarez, T.; Angelo, A. C. D.; DiSalvo, F. J.; Abruña, H. D. *J. Am. Chem. Soc.* **2004**, *126*, 4043–4049.

(16) de-los-Santos-Alvarez, N.; Alden, L. R.; Rus, E.; Wang, H.; DiSalvo, F. J.; Abruña, H. D. *J. Electroanal. Chem.* **2009**, *626*, 14–22.

(17) Cable, R. E.; Schaak, R. E. *Chem. Mater.* **2005**, *17*, 6835–6841.
(18) Leonard, B. M.; Bhuvanesh, N. S. P.; Schaak, R. E. *J. Am. Chem. Soc.* **2005**, *127*, 7326–7327.
(19) Schaak, R. E.; Sra, A. K.; Leonard, B. M.; Cable, R. E.; Bauer, J. C.; Han, Y. F.; Means, J.; Teizer, W.; Vasquez, Y.; Funck, E. S. *J. Am. Chem. Soc.* **2005**, *127*, 3506–3515.
(20) Sra, A. K.; Ewers, T. D.; Schaak, R. E. *Chem. Mater.* **2005**, *17*, 758–766.
(21) Volpe, D.; Casado-Rivera, E.; Alden, L.; Lind, C.; Hagerdon, K.; Downie, C.; Korzeniewski, C.; DiSalvo, F. J.; Abruña, H. D. *J. Electrochem. Soc.* **2004**, *151*, A971–A977.
(22) Ghosh, T.; Leonard, B. M.; Zhou, Q.; DiSalvo, F. J. *Chem. Mater.* **2010**, *22*, 2190–2202.
(23) Choi, J.-H.; Park, K.-W.; Kwon, B.-K.; Sung, Y.-E. *J. Electrochem. Soc.* **2003**, *150*, A973–A978.
(24) Deivaraj, T. C.; Chen, W. X.; Lee, J. Y. *J. Mater. Chem.* **2003**, *13*, 2555–2560.
(25) Drillet, J. F.; Ee, A.; Friedemann, J.; Kötz, R.; Schnyder, B.; Schmidt, V. M. *Electrochim. Acta* **2002**, *47*, 1983–1988.
(26) García-Contreras, M. A.; Fernández-Valverde, S. M.; Vargas-García, J. R.; Cortés-Jácome, M. A.; Toledo-Antonio, J. A.; Ángeles-Chavez, C. *Int. J. Hydrogen Energy* **2008**, *33*, 6672–6680.
(27) Lee, S.-A.; Park, K.-W.; Choi, J.-H.; Kwon, B.-K.; Sung, Y.-E. *J. Electroch. Soc.* **2002**, *149*, A1299–A1304.
(28) Travitsky, N.; Ripenbein, T.; Golodnitsky, D.; Rosenberg, Y.; Burshtein, L.; Peled, E. *J. Power Sources* **2006**, *161*, 782–789.
(29) Abu Bakar, N. H. H.; Bettahar, M. M.; Abu Bakar, M.; Monteverdi, S.; Ismail, J.; Alnot, M. *J. Catal.* **2009**, *265*, 63–71.
(30) Huber, G. W.; Shabaker, J. W.; Evans, S. T.; Dumesic, J. A. *Appl. Catal., B* **2006**, *62*, 226–235.
(31) Kim, H. J.; Choi, S. M.; Nam, S. H.; Seo, M. H.; Kim, W. B. *Catal. Today* **2009**, *146*, 9–14.
(32) Pawelec, B.; Damyanova, S.; Arishtirova, K.; Fierro, J. L. G.; Petrov, L. *Appl. Catal., A* **2007**, *323*, 188–201.
(33) Abdelsayed, V.; Aljarash, A.; El-Shall, M. S.; Al Othman, Z. A.; Alghamdi, A. H. *Chem. Mater.* **2009**, *21*, 2825–2834.
(34) Xiong, L.; Manthiram, A. *J. Electrochem. Soc.* **2005**, *152*, A697–A703.
(35) Adam, W.; Arce, J. *J. Org. Chem.* **1972**, *37*, 507–508.
(36) Murphy, D. W.; Christian, P. A. *Science* **1979**, *205*, 651–656.
(37) Chiu, H. W.; Kauzlarich, S. M. *Chem. Mater.* **2006**, *18*, 1023–1028.
(38) Prabakar, S.; Shiohara, A.; Hanada, S.; Fujioka, K.; Yamamoto, K.; Tilley, R. D. *Chem. Mater.* **2009**, *22*, 482–486.
(39) *Desk handbook: Phase diagrams for binary alloys*, illustrated edition; Okamoto, H., Ed.; ASM International.
(40) Gottfried, J. M.; Vestergaard, E. K.; Bera, P.; Campbell, C. T. *J. Phys. Chem. B* **2006**, *110*, 17539–17545.
(41) Wolter, O.; Willsau, J.; Heitbaum, J. *J. Electrochem. Soc.* **1985**, *132*, 1635–1638.
(42) Sadezky, A.; Muckenhuber, H.; Grothe, H.; Niessner, R.; Pöschl, U. *Carbon* **2005**, *43*, 1731–1742.
(43) Smith, G. P.; Boston, C. R.; Brynesta, J *J. Chem. Phys.* **1966**, *45*, 829–&.
(44) Smith, G. P.; Boston, C. R. *J. Chem. Phys.* **1965**, *43*, 4051–&.
(45) Brynesta., J; Boston, C. R.; Smith, G. P. *J. Chem. Phys.* **1967**, *47*, 3179-&.
(46) Gilman, S. *J. Phys. Chem.* **1964**, *68*, 2112–2119.
(47) Smith, S. P. E.; Abruña, H. D. *J. Phys. Chem. B* **1998**, *102*, 3506–3511.
(48) Schaefer, Z. L.; Ke, X.; Schiffer, P.; Schaak, R. E. *J. Phys. Chem. C* **2008**, *112*, 19846–19851.
(49) Tsai, Y. L.; Koel, B. E. *J. Phys. Chem.* **1997**, *101*, 2895–2906.